Pure appl. geophys. 163 (2006) 995–1019
0033–4553/06/060995–25
DOI 10.1007/s00024-006-0054-x

Pure and Applied Geophysics

Fracture in Westerly Granite under AE Feedback and Constant Strain Rate Loading: Nucleation, Quasi-static Propagation, and the Transition to Unstable Fracture Propagation

Ben D. Thompson,[1,2] R. Paul Young,[2] and David A. Lockner[3]

Abstract—New observations of fracture nucleation are presented from three triaxial compression experiments on intact samples of Westerly granite, using Acoustic Emission (AE) monitoring. By conducting the tests under different loading conditions, the fracture process is demonstrated for quasi-static fracture (under AE Feedback load), a slowly developing unstable fracture (loaded at a 'slow' constant strain rate of 2.5×10^{-6} /s) and an unstable fracture that develops near instantaneously (loaded at a 'fast' constant strain rate of 5×10^{-5} /s). By recording a continuous ultrasonic waveform during the critical period of fracture, the entire AE catalogue can be captured and the exact time of fracture defined. Under constant strain loading, three stages are observed: (1) An initial nucleation or stable growth phase at a rate of $\sim$ 1.3 mm/s, (2) a sudden increase to a constant or slowly accelerating propagation speed of $\sim$ 18 mm/s, and (3) unstable, accelerating propagation. In the $\sim$ 100 ms before rupture, the high level of AE activity (as seen on the continuous record) prevented the location of discrete AE events. A lower bound estimate of the average propagation velocity (using the time-to-rupture and the existing fracture length) suggests values of a few m/s. However from a low gain acoustic record, we infer that in the final few ms, the fracture propagation speed increased to 175 m/s. These results demonstrate similarities between fracture nucleation in intact rock and the nucleation of dynamic instabilities in stick slip experiments. It is suggested that the ability to constrain the size of an evolving fracture provides a crucial tool in further understanding the controls on fracture nucleation.

Key words: Shear-fracture, nucleation, earthquake, acoustic emission, rupture, granite.

1. Introduction

Shear failure of intact, brittle rock has long been experimentally investigated in order to better understand the mechanical properties of heterogeneous materials. In the case of earthquake physics, the presence of barriers or asperities is required on a pre-existing fault plane to store elastic strain energy which upon failure, generate strong motion seismic waves. The strength of these strong regions may approach that

[1]Department of Earth and Ocean Sciences, University Liverpool, Liverpool, UK
[2]Lassonde Institute, University Toronto, 170 College St, Toronto, ON, Canada.
E-mail: b.thompson@liv.ac.uk
[3]United States Geological Survey, Menlo Park, California, USA

of the intact material (OHNAKA, 2003). RECHES (1999) proposed that slip nucleation in earthquakes is analogous to rupture nucleation within an intact sample under triaxial conditions, based on: i) Field observations of fracture geometry complexity in fault zones, ii) partial or complete healing of crushed fault gouge at great depth, and iii) high values of energy release rate during earthquakes. OHNAKA (2003) considered earthquake rupture to be a mixed process of frictional slip failure and shear fracture of intact rock.

Previous AE studies have proven extremely useful in understanding brittle failure of rock. SCHOLZ (1968a) observed a temporal correlation between the onset of AE and dilation in a sample under triaxial loading, confirming the interpretation of BRACE *et al.* (1966) that dilation was caused by pervasive microcracking, primarily oriented parallel to the maximum compressive principal stress, σ_1. Insights have been provided into the nucleation phase of fracture, using AE source locations to map the temporal and spatial evolution of fracture. LOCKNER *et al.* (1991, 1992) slowed fracture to a quasi-static (stable) state using an AE feedback loading method, described by TEREDA *et al.* (1984). In the LOCKNER *et al.* study, AE source locations in granite were initially distributed uniformly throughout the sample, however close to peak stress, a clustering of AE occurred, forming a nucleus, from which fracture propagated as a process zone of intense activity. RECHES and LOCKNER (1994) and MOORE and LOCKNER (1995) used these experimental results to show that faults nucleate and propagate by the interaction of tensile microcracks. LEI *et al.* (2000) used a fast acquisition system to capture AE during triaxial tests on three hornblende schist samples under constant stress (creep) loading. In all tests, a fault nucleated close to the top of the sample and propagated through to cause rupture. The process zone is characterized as a region of intense tensile cracking, with the damaged fault zone behind this region characterized by shear events. LEI *et al.* (2003) also considered fracture initiation in samples with pre-existing planes of weakness. ZANG *et al.* (2000) used asymmetric uniaxial loading to propagate shear fracture in Aue granite. They examined fracture process zone characteristics using AE locations, and used AE first motion polarity to demonstrate that the predominant AE mechanism was shear-type cracking.

During periods of high AE activity, data sets collected using triggered AE systems can be incomplete due to system saturation. A continuous ultrasonic waveform acquisition system; the Giga RAM Recorder, has been developed to remove this limitation with the capacity to record a 268 s segment of waveform data on 16 channels (sampled at 5 MHz), typically about a significant occurrence, i.e., fracture of a sample. Discrete AE events are then extracted from this record, to provide the complete AE catalogue. In addition, the continuous record itself provides an extremely useful resource in terms of the timing of significant events in the experimental process, as demonstrated during stick slip tests by THOMPSON *et al.* (2005).

Although previous tests have demonstrated the characteristics of fracture nucleation in intact rock, the transition from nucleation to unstable fracture has not been clearly shown. Here, new observations of fracture are presented, which include a comparison of the nucleation of quasi-static and unstable fracture. Three experiments were performed in which fracture was induced in samples of Westerly granite under triaxial compression, using the same loading apparatus as LOCKNER *et al.* (1991). Firstly, the original LOCKNER *et al.* (1991) experiment was repeated, in which AE feedback loading was used to propagate a quasi-static fracture. Secondly, in order to demonstrate the evolution of unstable fracture, and the effect of loading rate on this process, two further tests were conducted under a relatively slow and a fast constant strain rate to demonstrate the evolution of shear fracture through the stages of nucleation, quasi-static (stable), and unstable propagation.

2. Experimental Procedure

2.1 Samples and Loading Conditions

Three triaxial compression tests are described featuring air-dried Westerly granite (cylindrical) samples with diameter 76.2 mm and length 190.5 mm. Sample ends were ground parallel to $\pm$ 0.05 mm. The grain size range of the samples is 0.05–2.2 mm, and a detailed description of the texture and microcrack morphology of Westerly granite can be found in MOORE and LOCKNER (1995). The samples were enclosed in a polyurethane jacket of thickness 3.2 mm, to prevent the entry of confining oil. Seventeen piezoelectric transducers were attached directly to the rock face with their surfaces ground to fit the curvature of the sample.

Testing was conducted at 50 MPa confining stress, with axial load being measured with an internal load cell to a precision of $\pm$ 0.02 MPa and axial shortening of the sample column measured outside the pressure vessel with a DCDT displacement transducer. In the first test, loading was controlled using an AE feedback loop to observe quasi-static fracture. In the second and third tests load was applied using constant piston displacement rates corresponding to constant axial strain rates of 2.5×10^{-6}/s and 5×10^{-5} /s. This was done to study the effect of loading rate on the onset of unstable fracture. These three experiments are hereafter referred to as the 'AEF' (AE Feedback), 'SL' (Slow Loaded) and 'FL' (Fast Loaded) tests.

The AE Feedback load control method was described by TERADA *et al.* (1984) and employed to provide AE source locations during quasi-static fracture propagation by LOCKNER *et al.* (1991). For the AEF test described in this paper, the procedure was software controlled. The AE rate was used to condition the computer-supplied reference voltage controlling the axial strain rate. The load control system was configured to maintain a constant rate of AE by reducing or reversing the axial

load in response to increased AE activity, therefore enabling the sample to be failed under quasi-static conditions. In the early stages of fracture propagation, rapid decreases in deviatoric stress were required to maintain the quasi-static state of the fracture. To facilitate this, axial load was controlled by a fast-acting hydraulic valve. The system response was approximately 0.2 Hz. As will be shown, altering the sensitivity of the AE feedback regime enabled the speed of fracture growth to be controlled at rates between 13–50 mm/hour. The quasi-static fracture state was maintained for approximately 14 hours.

2.2 Monitoring Acoustic Emission and Ultrasonic Velocities

The seventeen piezoelectric transducers used in the experiments had a radial mode resonant frequency of 0.4 MHz. Thirteen of these transducers were used as AE receivers, the remaining four were used as ultrasonic sources for velocity measurements. Additional details of the transducer response characteristics can be found in STANCHITS *et al.* (2003). The signal from the receivers passed through 40 dB external pre-amplifiers (PAC model 1220A). In addition, the signals from two receivers were split and also amplified using 20 dB amplifiers (within the Giga RAM Recorder) to provide a lower gain record of the experiment. The waveforms recorded during the SL test were observed to clip the $\pm$ 2.5 V amplitude scale during failure on the 20 dB channels and so one receiver was used to record an un-amplified (0 dB) signal for the FL test.

The Giga RAM Recorder, a novel AE acquisition system, enables recording of continuous ultrasonic waveforms for a significant period of time. This system records data on 16 channels, with two channels per acquisition card. Each acquisition card contains 5 GB of Random Access Memory (RAM), in total the RAM buffer is 40 GB. Data is digitized at 14-bit resolution and the input voltage range is $\pm$ 2.5 V. Data can be sampled between 2 and 40 MHz. Each board contains two 16 Kb First In First Out (FIFO) memories for discrete, triggered data, and two 20 dB amplifiers. The sampling frequency was 5 MHz for these experiments, providing a 268 s segment of continuous waveform data on 16 channels. The 40 GB RAM acts as a continuous circular buffer that can be 'locked' following the recording of a significant event, i.e., fracture of the sample, and subsequently transferred to disk. The system also records triggered data throughout testing, with identical parameters to the continuous data. A triggered event was recorded if five or more waveforms had amplitudes exceeding 100 mV in a 50 μs time window. Triggered events have a length of 204.8 μs, and a maximum of 16 events per second was captured. In addition, the number of AE per second was recorded throughout the experiment, this is termed the AE 'Hit' count to distinguish between this and the numbers of triggered AE actually recorded. Figure 1 shows a schematic diagram of the triaxial load configuration and acquisition modes of the Giga RAM Recorder.

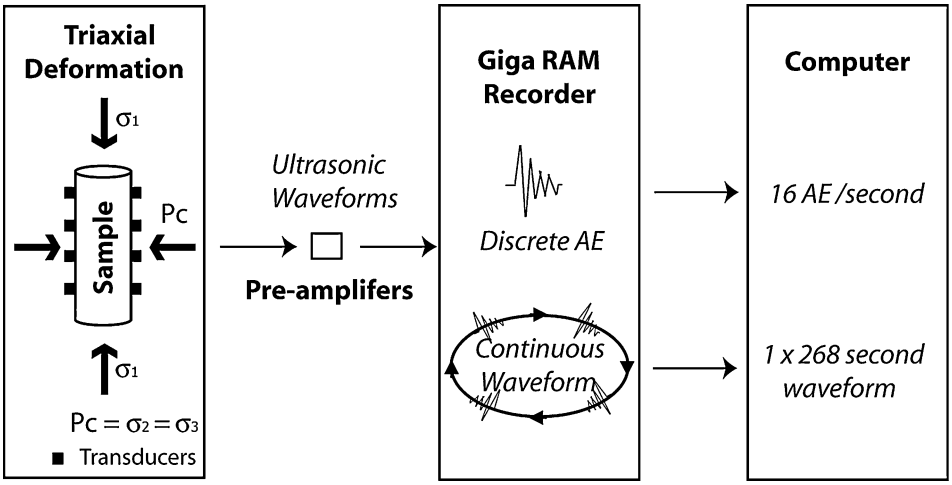

Figure 1
Schematic diagram of the experimental setup, including the triaxial load configuration and acquisition capabilities of the Giga RAM Recorder.

Following each experiment, the continuous ultrasonic record is replayed and the complete catalogue of discrete AE events is extracted using the trigger logic described above. Advances in technology have led to rapid AE waveform acquisition systems (LEI *et al.,* 2000). However, we believe this to be the first system to record continuous waveforms for significant time periods. The advantages of continuous waveform data include: (1) no 'mask' time, (i.e., the periods of recording downtime occurring when AE events are written to permanent storage), and (2) removal of the sampling bias imposed by trigger levels.

For ultrasonic velocity measurements, the four designated transducers were excited using a Panametrics (model 5072PR) pulse generator. A switch box rapidly connects the pulse generator to each source transducer. Stacked velocity surveys took 1–2 s to complete, with coverage along 52 raypaths.

2.3 AE Processing

P-wave first arrival times are obtained using an automated picking routine (ASC, 2003) and used to calculate AE source locations using a Simplex method (NELDER and MEAD, 1965). The residual difference between the measured and theoretical travel time from the source location is calculated for each channel, and if the residual exceeds 0.3 μs the channel is dropped from the location algorithm. Source locations calculated using fewer than 7 arrivals are not considered in this study. A Transversely Isotropic (TI) velocity structure was used in the location routine, defined by velocity measurements made throughout the experiments. An estimate of the average source

location error on the samples' surface is provided by location of the source transducers used in velocity surveys to within ± 4 mm of their true location. PETTITT (1998) theoretically considered the case of a cubic specimen (50 mm length) with velocity 4000 m/s and an array of 12 receivers, sampled at 10 MHz. AE were hypothetically located at the edge and in the center of the cube, and the location errors were analyzed as a function of position within the sensor array. AE at the center of the sample had between 25 and 50% smaller location errors than AE at the edge of the sample. It is probable therefore that our ± 4 mm measured error on the sample edge overestimates the location error within the sample by a similar amount.

2.4 b-values

The power-law frequency magnitude relationship is calculated using AE magnitudes M, corresponding to the Gutenberg-Richter b-value relationship for earthquakes (1):

$$\text{Log } N(M) = a - bM, \tag{1}$$

where N is the number of events greater than M, and a and b are constants. b is estimated using the least-squares method. The AE magnitude M is calculated for each located event as (2) and (3):

$$M = \log\left(\frac{\Sigma_{m=1}^{n}(W_{\text{RMS.d}_m})}{n}\right), \tag{2}$$

$$W_{\text{RMS}} = \sqrt{\frac{\Sigma_{i=1}^{x} W_i^2}{x}}, \tag{3}$$

where n is the number of sensors and d_m is the distance between receiver m and the AE location. W_{RMS} is the RMS waveform amplitude calculated on each receiver, using the waveform amplitude $W_{i,}$ averaged over x data points. In the Earth, typically b ranges between 0.5 and 1.5 (VON SEGGERN, 1980).

3. Results

3.1 Mechanical Behavior

The mechanical data for the three tests are plotted in Figure 2. Figures 2a–c show the deviatoric stress (σ_1-P_c) versus time with cumulative AE count plotted on the secondary axis, for the AEF, the SL and FL experiments, respectively. Figure 2d shows the deviatoric stress versus axial strain measurements for the three experiments.

The AEF test (Fig. 2a) can be summarised as follows:

(Approximate times are given in minutes, exact timing in seconds)

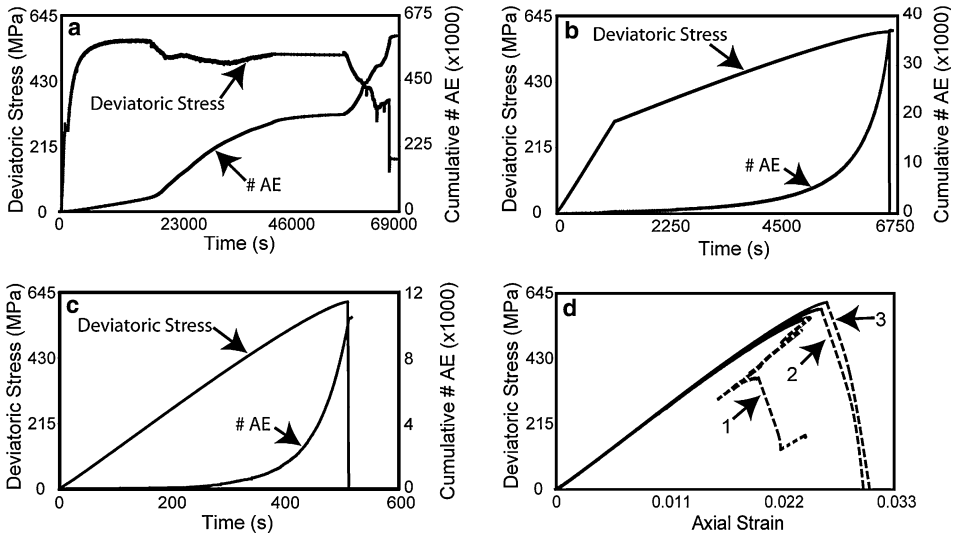

Figure 2
(a–c) Deviatoric stress and AE Hit count versus time for tests under the following load control methods: (a) AE Feedback (AEF), (b) slow constant strain rate (2.5×10^{-6}/s) (SL) and (c) fast constant strain rate (5×10^{-5}/s strain rate) (FL). (d) Deviatoric stress versus axial strain curves for the AEF (marked 1), SL (2) and FL (3) tests, with the unloading portions of the curves dashed.

1) Initial loading under a constant strain rate of 1×10^{-5}/s until approximately 390 MPa. From this point, the loading rate is moderated by the AE. The kink in stress curve at 800 s occurred when a velocity survey interfered with the AE feedback control. Such loading anomalies were subsequently avoided by momentarily turning off the AE feedback control prior to velocity surveys.
2) At 182 minutes (10889 s) a deviatoric stress 'plateau' was reached (560 MPa).
3) Peak stress (564 MPa) was reached after 260 minutes (15579 s). There was then a gradual stress drop to 559 MPa (18575 s).
4) The stress then drops at an approximate rate of 0.2 MPa per second to a minimum of 504 MPa after 358 minutes (21500 s).
5) Between 731 minutes (43869 s) and 979 minutes (58765 s) a constant axial strain of 0.0236 was maintained as the equipment was unattended.
6) The AE feedback control was restarted at 979 minutes (58765 s) and periodically adjusted to increase the speed of fracture propagation.
7) Finally at 1132 minutes (67936 s) the AE Feedback regime was adjusted to accelerate the fracture rate and the fracture became unstable and propagated completely through the sample, resulting in a 195 MPa stress drop.

The sample in the SL test (Fig. 2b) was loaded at an initial axial strain rate of 1×10^{-5}/s to 300 MPa to approximately 50 percent of failure stress and then reduced to 2.5×10^{-6}/s. The AE hit count increased exponentially towards failure, the peak

stress of 592 MPa was reached after 6549 s. There was a 38 s period of strain weakening, after which the stress dropped abruptly. Hardware problems caused a periodic loss of AE location data up to failure, but fortunately this problem did not affect the final 21 s in which strain weakening and dynamic fracture occurred. The AE hit count was unaffected by the hardware problem and 35,000 AE hits were registered.

The FL test was loaded at a strain rate of 5×10^{-5}/s (20 times faster than the SL experiment), reaching the peak deviatoric stress of 615 MPa after 510 s. In this case, fracture ensued immediately without a period of strain weakening. Over 11,000 AE hits were recorded, compared with 35,000 during the SL test, and close to 500,000 during the AEF test. Total stress drops were experienced for both the SL and FL samples.

3.2 Velocity Data

Fourteen velocity surveys were conducted for the AEF test, constraining the evolution of damage within the sample. Initially, at the onset of deviatoric loading, maximum and minimum velocities were 6070 ± 83 and 5602 ± 83 m/s, respectively (7.7 % anisotropy). Under deviatoric loading, a TI structure evolves, as shown in Figure 3a, where velocity is plotted as a function of raypath angle at intervals during the test. For clarity, only six of the fourteen surveys are plotted. The TI structure can be modelled by:

$$V(\theta) = ((V_{\max} + V_{\min})/2) - ((V_{\max} - V_{\min})/2)\cos(180 - 2\theta)), \tag{4}$$

where V is modelled P-wave velocity as a function of raypath angle, θ, and $V_{\max}$ and $V_{\min}$ are the maximum and minimum P-wave velocities. Velocity models of the form (4) are fitted to the measured velocity data and used to define the TI structure input into the AE source location routine. Figure 3b shows a similar plot for the SL test with four velocity models estimated between deviatoric stresses of 425 and 545 MPa. Fewer velocity surveys were conducted due to the relatively shorter period of the test. Indeed, the duration of the FL test meant surveys were only conducted up to 69% peak stress, these data are not shown. In Figure 3c, the percentage of anisotropy derived from the TI velocity models is plotted as a function of deviatoric stress for the AEF and SL tests. The two curves display close similarity. Between 350 MPa and 500 MPa there is a linear increase in anisotropy from 8% to 19%, from which point the increase appears nonlinear. By 545 MPa, the samples are 26% anisotropic, above which measurements only exist for the AEF test. At peak stress, the sample exhibits 35% anisotropy. The evolution of velocity for this test is simplified in Figure 4i, where the averaged velocity for four horizontal ray-paths is shown as a function of deviatoric stress and time. The TI data from the AEF test are used by SCHUBNEL *et al.* (this volume) to demonstrate the evolution of crack density in Westerly granite.

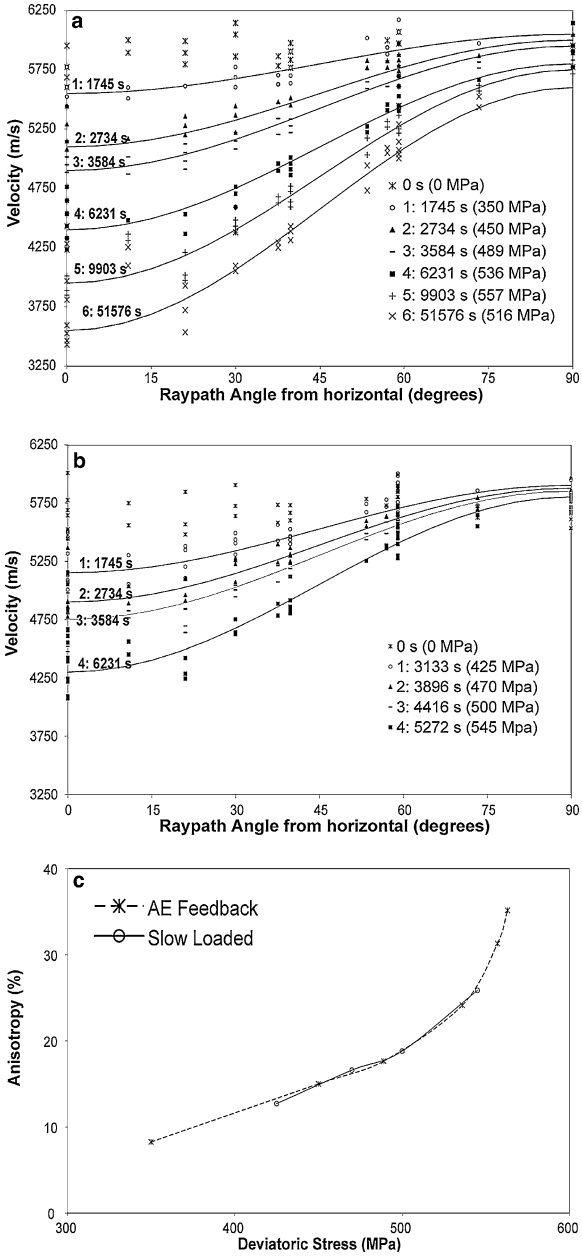

Figure 3

The evolution of the Transversely Isotropic velocity structures for (a) the AEF and (b) the SL test. Data points represent measured velocities as a function of raypath angle, measured from the horizontal, for a series of velocity surveys conducted at increasing deviatoric stresses (as marked, time of survey is also indicated). Velocity models are fitted to the data points (models are not fitted to the initial surveys), as detailed in the text. (c) The percentage anisotropy derived from the velocity models is plotted against deviatoric stress for these two tests, indicating a similar degree of damage was induced in the samples as a function of deviatoric stress.

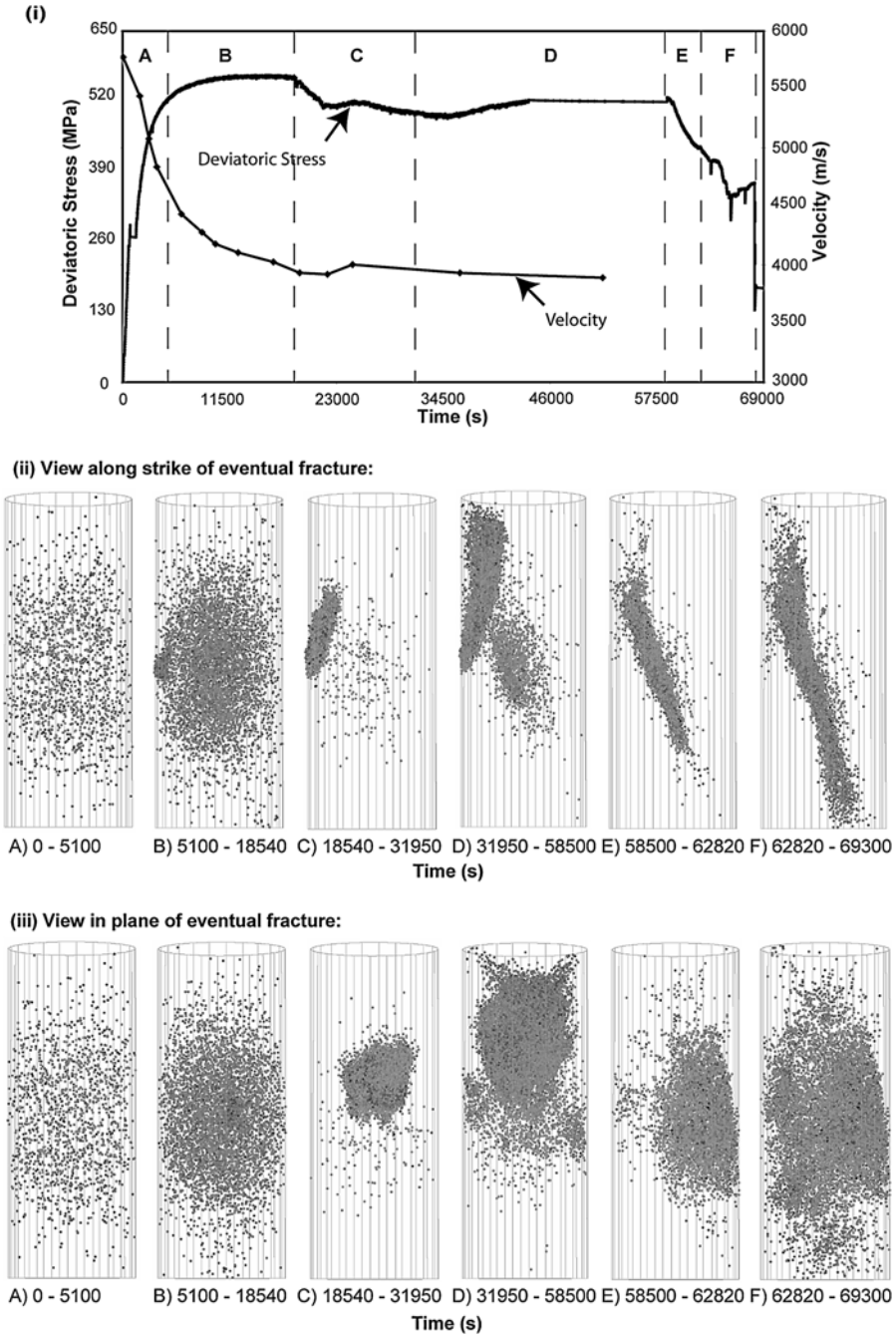

Figure 4

(i) Deviatoric stress and average velocity (measured along four horizontal raypaths) during the AEF test, with time. AE locations are shown looking along the strike of the first fracture (ii), and into the plane of the eventual fracture. Periods A–F are marked on (i).

3.3 AE Locations

Over 70,000 triggered AE were located from the AEF test, and are presented in Figure 4. The locations are divided into six periods (A–F), as marked on Figure 4i. AE locations are shown along the approximate strike of the first fracture plane (Fig. 4ii), and secondly, perpendicular to the strike of the first fracture plane (Fig. 4iii). In Period A, AE locations are distributed throughout the sample. In Period B events are still distributed throughout the sample, however there is also a clustering at the edge of the sample. Period C shows a fracture which propagates from the nucleation site. Few events are located elsewhere in the sample. In Period D, the fracture has reached the top of the sample, intersecting the steel platen. The initial angle of the fracture is 70°, this steepens as the fracture propagates towards the loading platen, and reacts to the more complicated stress field produced by this nearly rigid boundary. A second fracture is then observed to nucleate and propagate (Periods D to F). The second fracture is shown in greater detail in Figure 5. The first fracture grows at an average rate of 12 mm/hour (3 μm/s) while the rate of growth for the second fracture was increased from 12 to 50 mm/hour (3 to 14 μm/s), by reducing the sensitivity of the AE feedback control.

For the SL and FL tests the AE events presented are extracted from the continuous record. The triggered events occurring outside the continuous record are not considered in this paper, although it is noted they show a similar distribution to events in the early stages of the AEF. A continuous waveform is shown in Figure 6i, including a 22 s period which includes rupture for the SL experiment, during which time the sample exhibits strain-weakening behavior. Periods A to E on the continuous waveform define the times for which AE locations are displayed. Region YY' is expanded to show a 0.8 s period about failure. A 40 ms region of this waveform is again expanded (ZZ') showing details of failure. 2100 events were located during the final 21 s of the SL test and are displayed in five time periods. Views are shown along strike of the eventual fracture plane (Fig. 6ii), and into the plane of the eventual fracture (Fig. 6iii). In Periods A and B events cluster on the sample edge. In Period C the cluster zone has grown slightly, and in Period D significant growth is observed. In Period E, AE are used to estimate the length of the fracture as 52 mm. These are the last AE that can be located, and the time of the last located AE is marked on the continuous record (Fig. 6i, Z-Z'). The continuous record shows a gradual rise in amplitude from this point, and 17 ms after the last AE located, the 2.5 V amplitude scale continuously clips, for a period of 6 ms. During this period, rupture is assumed to occur. Following rupture, there is approximately 200 ms of relative quiescence prior to large amplitude aftershocks.

A summary of continuous waveform for the final 178 s of the FL test is displayed in Figure 7i, and the final four seconds are expanded in waveform Z-Z'. Similar to the SL test, a rapid increase in activity is observed a few seconds before failure. 2700 AE are located from the continuous record and displayed for Periods A–E, as

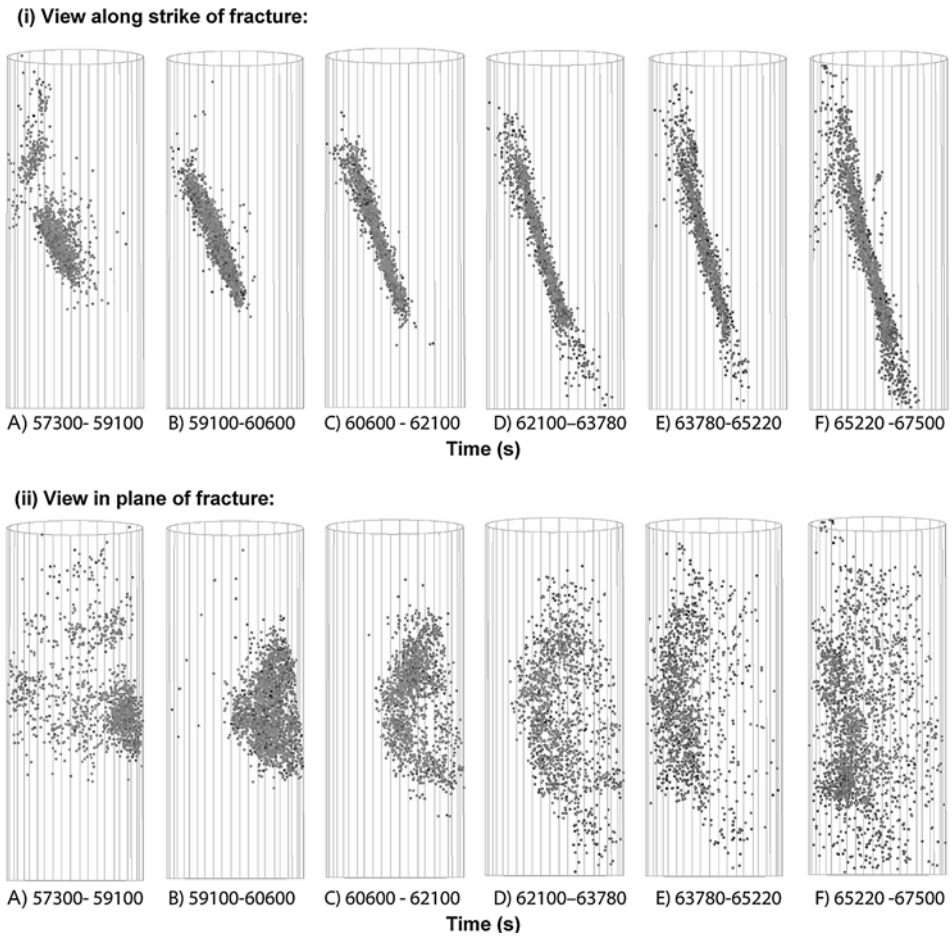

Figure 5
Detail of the second fracture propagating in the AEF test. The fracture nucleates and propagates as a process zone of intense activity.

marked in Figure 7i. In Periods A and B events are distributed throughout the sample. In Period C, events are also distributed throughout the sample, with a cluster of events developed in the center of the sample. In Period D, this cluster develops further. Period E shows the final AE before rupture. The AE is concentrated in two areas; firstly in the center of the sample, and secondly, a new cluster has developed on the edge of the sample. The fault angle and a physical examination of the sample indicate this second cluster is the source of the macro-fracture. Figure 8a is a continuous waveform showing a 262 ms period about failure, expanded from Figure 7i. The last AE locates at 510.164 s. For this experiment only, an unamplified

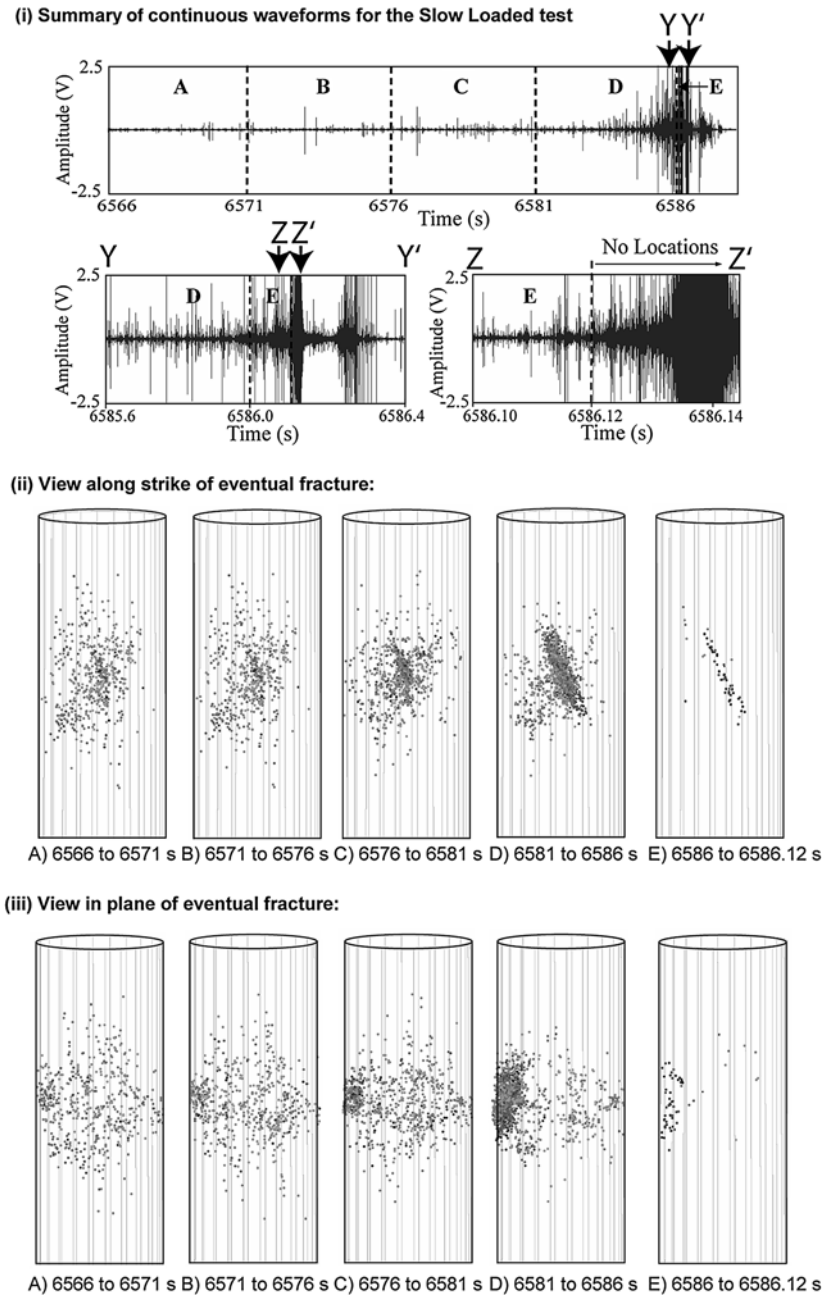

Figure 6

Slow Loaded Test: (i) the continuous waveform is summarized for a 20 dB channel for a 22 s period. The period marked Y to Y' is expanded, showing 0.8 s of detail about the failure. The period marked Z to Z' is expanded, showing in greater detail a 40 ms period of failure. (ii–iii), AE locations for the 21 s period prior to failure are shown with location periods A–E marked on the continuous record. Following E, there is a short time prior to the sample rupture during which no locations are possible.

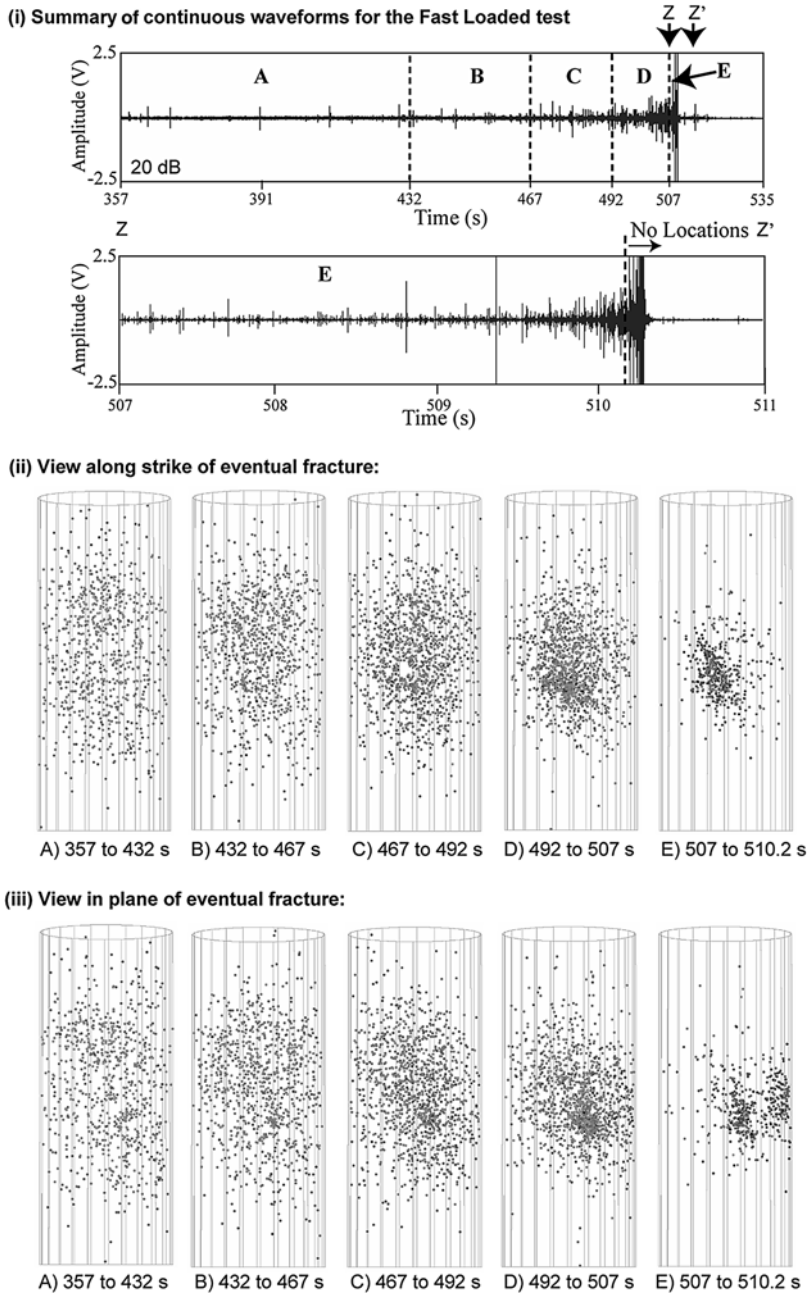

Figure 7

Fast Loaded Test: (i) the continuous waveform is summarized for a 20 dB channel for a 178 s period. The period marked Z to Z' is expanded, showing 4 s of detail about the failure. This region is further expanded in Figure 8. (ii-iii) AE locations for the 153.2 s period prior to failure are shown with location periods A-E marked on the continuous record. Following E, there is a short time prior to the sample rupture during which no locations are possible.

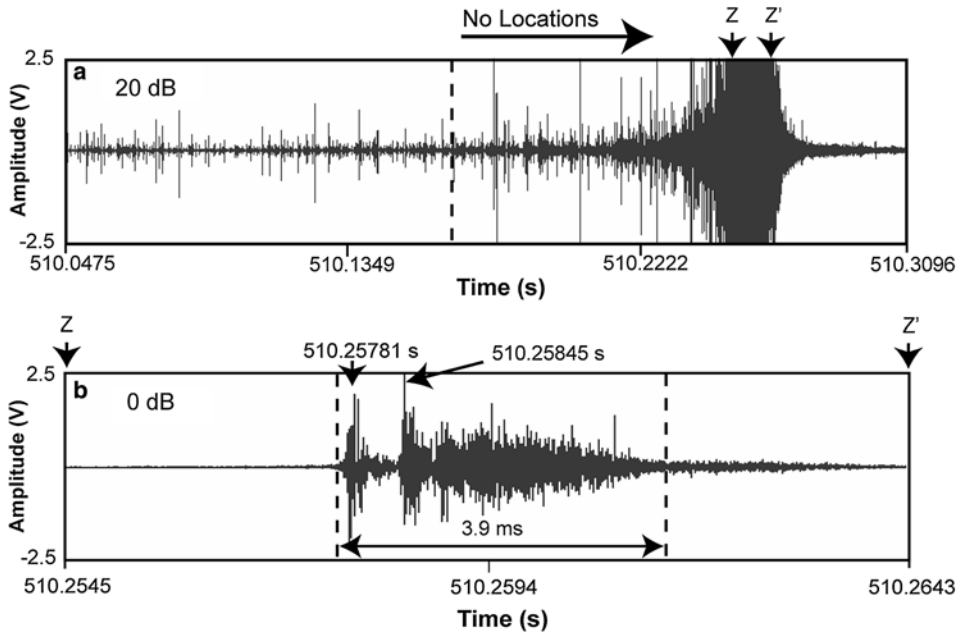

Figure 8
Continuous Waveform for Fast Loaded Test, expanded from Figure 7i to show detail of fracture. a) The amplitude scale of the 20 dB channel saturates, however on the 0 dB channel (b) the ultrasonic response of failure is unclipped. In (b), two pulses are observed over a 3.9 ms period, the point of sample rupture is interpreted to coincide with the maximum amplitude at 510.2585 s. The timing of waveform Z-Z' (b) is indicated on (a).

(0 dB) transducer recorded failure and Figure 8b shows the response for this channel. There are two pulses or bursts of activity: the first of which lasts 0.3 ms. The onset of the second is approximately 0.6 ms after the onset of the first. The point of highest energy release is at 510.2585 s and is assumed to represent the time of failure. From this we conclude that the final AE locates approximately 100 ms prior to rupture.

3.4 b-values

The *b*-values calculated for the three experiments are presented in Figure 9, along with deviatoric stress and time. *b*-values for the SL and FL tests were calculated using 400 event samples. Figure 9i shows results for the AEF test, calculated using 400 event samples until fracture propagation, and using 1000 event samples after this point (due to the large amount of data). Between 14,285 and 21,312 s, *b*-values are calculated using both 400 and 1000 event samples. The trends are nearly indistinguishable, which demonstrates that in this case, varying the sample size does not affect the results presented. *b*-values are initially about 2.5 $\pm$ 0.3. There is a

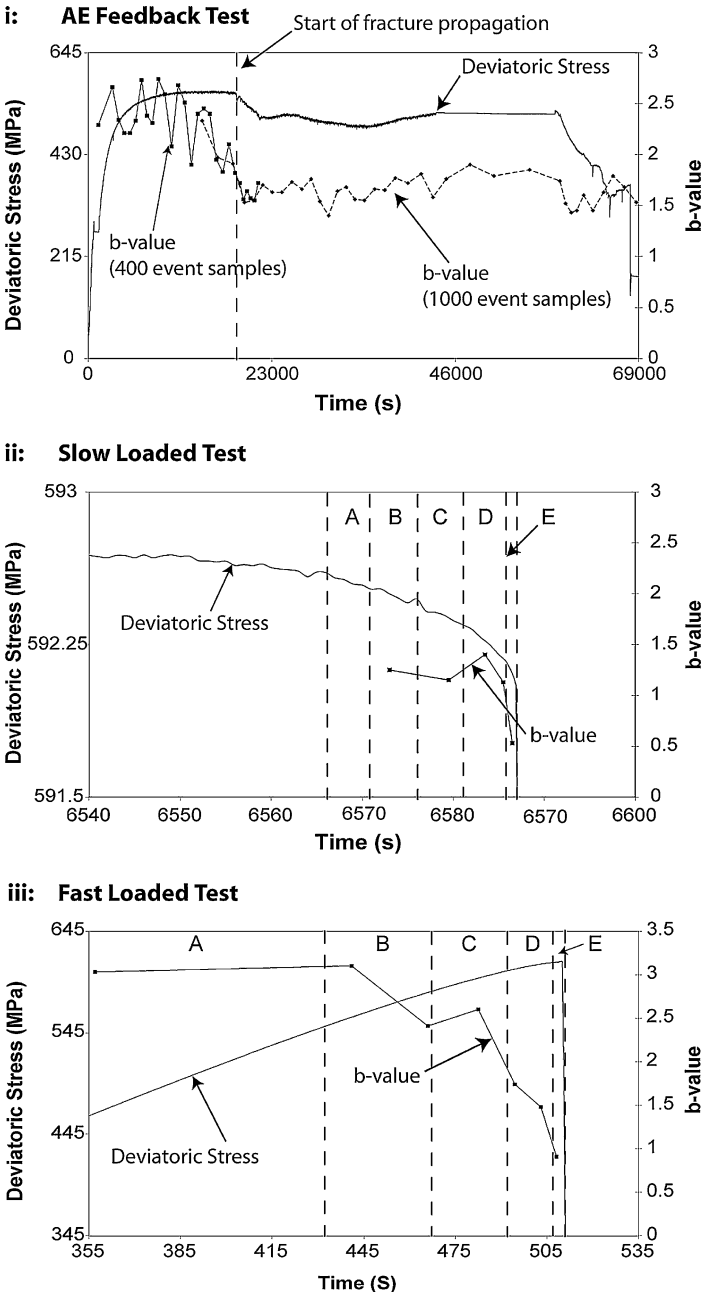

Figure 9
b-values marked with deviatoric stress and time for the three tests. The moment of fracture propagation is marked on the AEF test (i), and the 400 and 1000 event sample sizes show close agreement around this period. It is practical to use large event bin sizes for the duration of the AEF test, however, a comparison is provided for the SL (ii) and FL Tests (iii) by calculating b-values using smaller 400 event bins up to nucleation of fracture. A to E on (ii) correspond to the AE location periods for the SL Test in Figure 6, and A to E on (iii) correspond to AE location periods for the FL Test in Figure 7.

gradual decrease in the average *b*-value with increasing stress. The start of fracture propagation is marked by a dashed line in Figure 9i, from which point the large fluctuations observed in the *b*-value trend are not observed. The *b*-value reaches a low of 1.53 following the initial stress drop (21500 s). From this point until the end of the test the average *b*-value is 1.69.

The *b*-values from the SL test are shown in Figure 9ii, along with the deviatoric stress record for the 60 s period about failure. *b*-values average 1.23, decreasing suddenly to 0.53 about failure. *b*-values for the FL test are shown in Figure 9iii. Initially *b*-values are above 3. From 482 s there is a near linear decrease to a final *b*-value of 0.91.

4. Nucleation of Unstable Fracture

AE locations from the SL and FL tests demonstrate fracture nucleation, and the initial propagation of a fracture. The continuous record is used to estimate the time of sample rupture, which is assumed to be the point of highest amplitude. For the FL test, the 0 dB channel recorded the maximum amplitude at 510.2585 s, which is 1.2 ms after the ± 2.5 V amplitude scale continuously clipped on the 20 dB amplified channels. We assume that the point of rupture for the SL test (which did not feature a 0 dB channel) occurred approximately 1.2 ms after saturation of the 20 dB channels, i.e., at 6586.138 s (the potential errors associated with this assumption are considered later).

Having estimated the time of sample rupture, we will demonstrate the spatial and temporal evolution of nucleation and initial fracture propagation with respect to this event for the constant strain rate tests. To provide accurate measurements of fault growth, AE location coordinates (X,Y,Z) are rotated so the new Y axis is oriented along the strike of the fracture. This is shown in Figure 10. AE locations only in the immediate region defined by the respective fracture zones are considered. The length of the fracture (defined as the long axis of the main AE cluster) is directly measured. For the SL test, 600 events are sequentially displayed in samples of 100 (Fig. 10a) while in the FL test, four groups of 25 events are displayed (Fig. 10b). In order to provide a time resolution for Figure 10, each subsequent sample is stepped along the horizontal (X) axis, by 15 mm per sample for the SL test, and 25 mm per sample for the FL test. The nucleation or fracture zone is shaded and was visually estimated as the zone of dense AE activity for each sample of events. For each nucleation or fracture zone the long axis is measured using the coordinates of the two outlying AE locations. Figure 11a shows the measured fracture length with time (the time of the final AE located in that sample of events). Figure 11b is plotted using a logarithmic time scale in order to emphasize the length-time relationship in the second prior to dynamic fracture. The interpreted stages of fracture are illustrated for the SL test (as defined in the discussion).

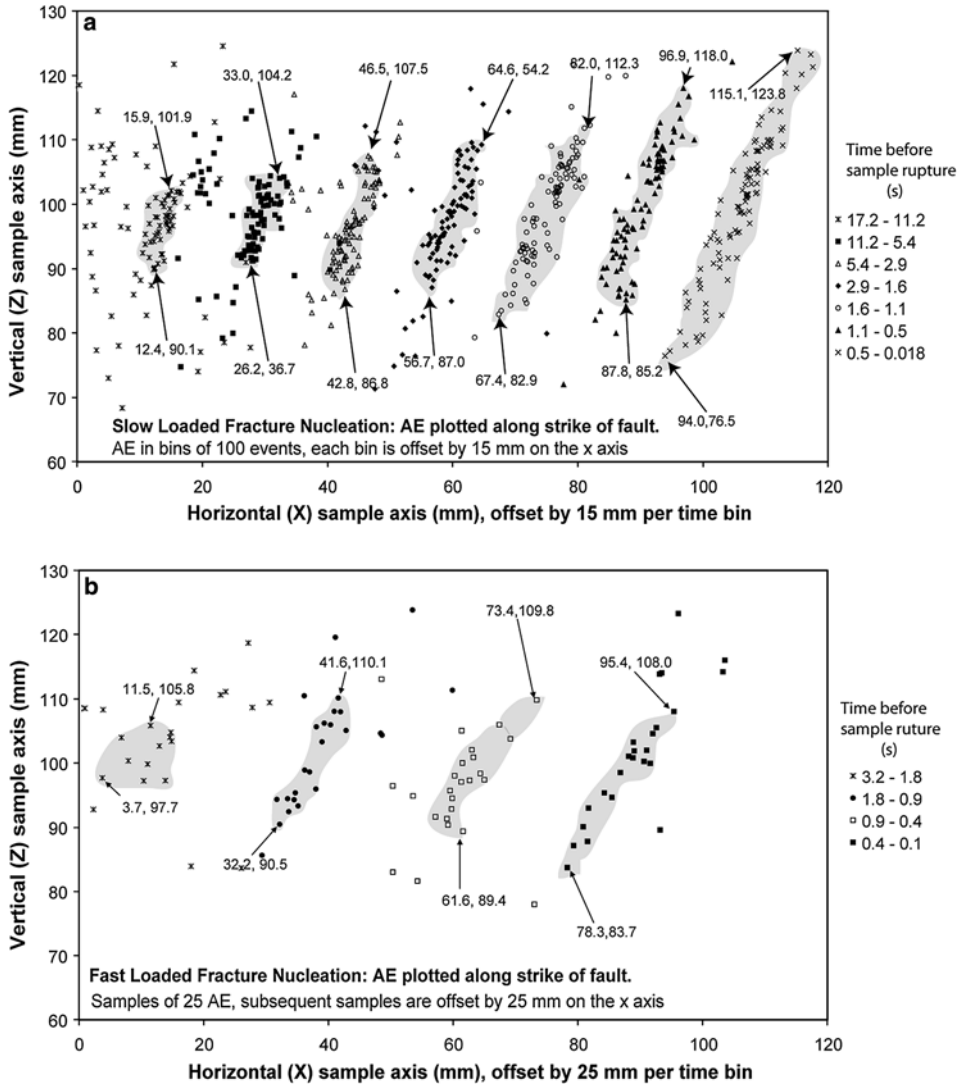

Figure 10
Comparison of Nucleation/Fault Length for the SL (a) and FL (b) tests. AE coordinates (X,Y,Z) are rotated so the Y axis is aligned with the strike of the eventual fault plane, and plotted for the rotated X and Z axes. Time resolution is provided by stepping each event bin along the X axis by 15 or 25 mm (for the SL and FL Tests respectively). The time prior to sample rupture for each group of AE is indicated.

For the SL test, nucleation can be accurately defined from AE locations between 17.2 and 11.2 s prior to rupture of the sample. It is possible that the nucleation zone existed before 17.2 s, however it is difficult to define from the AE locations. At 11.2 s the initial length is 11 mm, which slowly increases to 24 mm, 1.62 s prior to rupture

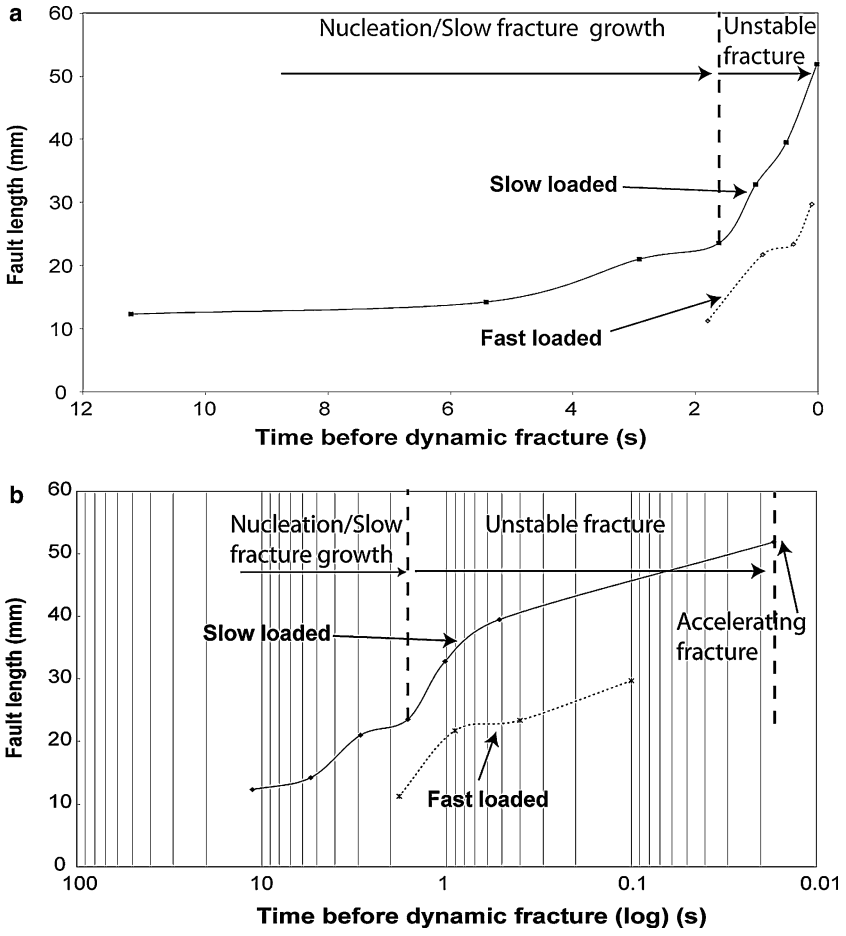

Figure 11
Nucleation or fracture lengths inferred from Figure 10 are plotted (a) against time prior to sample rupture for the FL and SL tests. (b) A logarithmic time scale is used to emphasize the differences between the two tests immediately prior to the dynamic rupture, the timing of which is inferred from the continuous records. The interpreted stages of nucleation and fracture growth are marked for the SL test.

(a rate of 1.3 mm/s). The fracture is then measured to grow at 17.7 mm/s until 18 ms prior to rupture, when the fracture length is 52 mm.

For the FL test, nucleation is observed between 3.2 and 1.8 s prior to the sample rupture, with an approximate diameter of 11 mm. The fracture evolves into a planar feature in the period 1.8 and 0.9 s before rupture. There is a small increase in fault length between 0.9 and 0.4 s before rupture. At 100 ms before rupture, the fracture length increases to a length of 30 mm at an average velocity of 21 mm/s. No events are located between 100 ms and the sample rupture. The inability to locate further AE in the SL and FL tests is due to an increase in activity in the sample, as when

many events occur in a short time period, AE first arrivals are masked by the coda of earlier events.

5. Discussion

In the previous section AE locations are used to define a propagating fracture. At a critical point, no AE are located due to the high level of activity in the sample. This occurs 18 and 100 millisecond periods prior to fracture, for the SL and FL tests respectively. An important question is what happens to the fracture growth in this final period in which no AE locations are possible? The simplest explanation is that the increased AE activity preventing source location is purely a function of the larger fault size, and that the length of the fault continues to grow at 17.7 mm/s (in the SL test). This is discounted by a simple calculation of average velocities required for the fault to reach the sample dimensions (which is 136 mm, taking the final 56° fracture angle measured from Figure 10a). Given that the fault must grow a further 84 mm over a period of 18 ms, the average velocity must accelerate to 4.7 m/s. This value is based on the assumption that similar to the FL test, rupture occurs 1.2 ms after the 20 dB waveform continuously clips, with the continuous clipping persisting for 6 ms. If rupture occurred later, i.e., midway through the clipped period, the 21 ms propagation period would suggest a 4.0 m/s average velocity. To illustrate the extreme case, if rupture occurred at the end of the clipped period, then the 24 ms propagation period would suggest an average velocity of 3.5 m/s. However, it would seem counterintuitive for rupture to coincide with unclipping of the waveform and the fracture rate is thought to be in the 4.0 m/s to 4.7 m/s range. Furthermore, it is emphasized that these estimates represent the average fracture velocity over the final $\sim$20 ms rather than the ultimate propagation velocity.

In the case of the FL test, the fracture is required to propagate a further 106 mm in 100 ms, requiring acceleration to an average velocity of 1.0 m/s. However in this case the unclipped waveform offers further evidence. As shown on Figure 8b, there is an initial pulse followed by a second, higher magnitude pulse with longer duration, occurring 0.6 ms after the onset of the first. It would be plausible to assume the first represents the onset of dynamic fracture, and the second the point at which the fracture has completed its growth phase and slip occurs on the entire fault. Indeed, fracture mechanics analysis (RICE, 1980) and microstructural analysis of a quasi-statically propagated fault (MOORE and LOCKNER, 1995) suggest that for a crack propagating into unfractured rock, there is very little net slip on the fault behind the fracture tip, with the unbroken rock ahead of the fracture resisting the applied load. However, once the fracture has propagated completely, only the frictional resistance remains and slip on the entire fault plane occurs as in a spring-slider system. Such slip will involve considerable AE activity, as observed by the larger magnitude and duration of the second pulse. Assuming that the fault continues to accelerate at 21 mm/s between the

last locatable AE and the unstable propagation (a period of 0.1 s), the fault will have a length 31 mm. A further growth of 105 mm is required, which must then occur in the 0.6 ms period between the onset of the first and second pulse. This suggests the average unstable fracture speed is 175 m/s. High resolution strain measurements will be employed to test the assumptions involved in this calculation.

The fracture process observed for the SL test is interpreted as a three stage process. Firstly, a nucleation or slow growth stage is observed to extend at an average velocity of 1.3 mm/s. Secondly, the nucleating fracture reaches a critical size or propagation velocity and a sudden increase in propagation velocity to 17.7 mm/s is observed. It is beyond the resolution of the techniques used here to determine whether the velocity is constant or accelerating in this stage. As acceleration in stress drop is observed (Fig. 9ii) we infer that the fracture could not be halted at this stage even with a release in the applied load, and so we interpret this stage as unstable fracture. The third stage occurs after the final AE locates, when it is demonstrated that acceleration in propagation speed to the order of m/s must occur. The interpreted stages of nucleation and fracture growth are marked on Figure 11. In the FL test, failure occurs at peak stress, i.e., strain weakening is not observed. We consider that the process observed over 17 s for the Slow Loaded test is accelerated into a period of 3 s for the Fast Loaded test. Furthermore, by taking into account the additional constraints of the unclipped waveform about fracture for the FL test, it is suggested that the final unstable velocity is approximately 175 m/s.

These observations can be compared to an earthquake nucleation model proposed by OHNAKA (2000), based upon results from stick slip experiments conducted on preexisting fault planes under biaxial loading, (OHNAKA and SHEN, 1999). In the first phase of this model, rupture nucleation initially proceeds stably and quasi-statically to a critical length, the second phase is a spontaneous acceleration of the nucleation to a second critical length, from which point rupture will extend at a constant velocity close to the shear-wave velocity (phase 3). Indeed OHNAKA (2003) links fracture initiation, frictional slip, and earthquake nucleation in a constitutive law. To apply our observations to this model; the first and sudden acceleration in fracture speed when the fracture length reached 24 mm would correspond to the critical length (or propagation velocity) above which the fracture becomes unstable. Similarly, the 52 mm fracture length at the point from which AE were not located represents a lower bound of the critical dimension (or propagation rate) above which the final propagation velocity ($\sim$ 175 m/s) is reached. That the suggested ultimate propagation velocity is lower than that of the shear wave-velocity, may be due to the limited sample size in these tests.

LEI *et al.* (2000) demonstrated the processes of fracture under constant stress (creep) loading using a fast AE acquisition system. They observed two stages of nucleation with nucleation initially growing to a size of 2 cm at a speed of 3 cm/s. There was then a pause in growth for 12 s, while activity in this area continued. The nucleating fault then grew to the edge of the sample at 10 cm/s. A 2 s delay ensued

before the sample rupture occurred. There are differences between LEI *et al.*'s observations and those presented here; specifically the complete propagation of the nucleating fracture, its rapid propagation rate and the two-second pause between propagation and rupture were not observed in our experiments. There are possible reasons for these discrepancies. Firstly, the loading rate may influence the critical fault dimensions (or propagation rate) above which fracture propagates at velocities of order m/s, causing a larger critical size above which an accelerating fault is observed. Secondly the sample size may be an issue as those used in this study are larger, with a length of 190.5 millimeters compared to 100 millimeters used by LEI *et al.*, with an aspect ratio of 2.5:1 compared to 2:1 in their experiments. Use of a larger aspect ratio increases the region in the center of the sample that has low stress gradients (MOGI, 1962; PATERSON and WONG, 2005) and can help reduce problems related to end effects. Unlike in LEI *et al.*'s experiments, we find fracture nucleates consistently away from the loading platens. It could be that the fracture processes are complicated by stress concentrations when nucleation occurs close to the loading platen. Separating the relative importance of these geometrical differences from differences in loading conditions (i.e., constant strain rate versus constant stress) will require additional experiments.

The nucleation prior to quasi-static propagation in the AE feedback test is measured to have an approximate long axis of 18 mm. This is close to the 24 mm fault length prior to the 17 mm/s propagation measured for the SL test, and is consistent with that previously measured in AE feedback tests (LOCKNER *et al.*, 1991) and creep tests (LOCKNER and BYERLEE, 1980) on Westerly granite, and by LEI *et al.*, (2000). Therefore, we conclude that the initial nucleation size of fracture initiation under these experimental conditions is not greatly influenced by the loading rate, and it is in the initial propagation stage that the fracture characteristics diverge according to loading rate.

SCHOLZ (1968b) demonstrated that *b*-values were negatively correlated with the level of applied stress. MAIN and MEREDITH (1989) related intermediate and short-term *b*-value anomalies to stress intensity during fracture. LEI *et al.* (2000) concluded that variations in *b*-value occurred as result of hierarchical fault growth. The *b*-values presented here are broadly similar to LEI *et al.*'s experimental results, although *b*-values during quasi-static fracture propagation have not previously been measured over an extended period (i.e., AEF). For this test, the *b*-values fall to about 1.5 to coincide with stable fracture propagation. For the FL test, the *b*-values fall to about 1, however in this case large events are masking smaller events, lowering the measured *b*-value. For the SL test, locations are only shown for the post peak region of the test, and therefore nucleation has already developed, explaining the initial *b*-value of between 1 and 1.5. However as the fracture develops, the *b*-value falls to 0.5, which is a value associated with earthquake foreshock nucleation (VON SEGGERN, 1980).

6. Conclusion

This paper presents results of three triaxial compression tests in which the process of fracture nucleation is compared under AE Feedback, and 'Slow' and 'Fast' constant strain rate loading. A continuous ultrasonic waveform recorder was used to capture the entire AE catalogue about failure, and this continuous waveform enables the exact time of rupture to be estimated. By repeating the AE feedback controlled test of LOCKNER *et al.* (1991), quasi-static fracture is propagated through a sample over 14 hours, at rates of between 3 and 14 μm/s. As shown by LOCKNER *et al.*, fracture nucleates at a site of intense cracking, at the side of the sample, and propagates through the sample as a process zone of intense activity.

By loading under a constant strain rate, the evolution of unstable fracture nucleation has been demonstrated. Firstly, a slowly expanding nucleation site is observed, followed by a sudden increase in fracture speed (to mm/s or cm/s) up to a size (or propagation rate) above which AE are not located. A lower bound estimate of the propagation velocity from this point (using the time-to-rupture, the existing fracture length, and assuming a constant velocity) suggests values of a few m/s. However, from the low gain acoustic record, we infer that the final speed of rupture propagation had increased to hundreds of meters per second. For both slow and fast constant strain loaded experiments, we observe a monotonically increasing fracture growth rate similar to behavior predicted by avalanche models for fault growth.

It is accepted that earthquake physics can be modelled largely as a frictional process, but in situations where nucleation occurs in fault step-overs and on nonplanar surfaces at high normal stresses, earthquake occurrence may involve a component of rock fracture. Indeed, under special circumstances, such as in some mining-induced earthquakes, nucleation and initial propagation may occur entirely in intact rock. Here we have shown there are similarities between the nucleation of dynamic instabilities during intact rock failure and frictional instabilities on pre-existing fault planes in the laboratory. The critical dimensions of the nucleating fault at the transition to unstable rupture appear to be easily observed under the experimental conditions described here, using continuous AE recording. It is suggested that a better understanding of the controls on fracture nucleation, and the transition to unstable rupture in the laboratory could improve the understanding of earthquake nucleation.

Acknowledgments

We thank A. Schubnel, D. Collins, R. Bowes (Engineering Seismology Group, Inc.) W. Pettitt (Applied Seismology Consultants, Ltd.), A. McGarr and N. Beeler for helpful discussions, and A. Zang and X-L. Lei for useful reviews. This work was

made possible by a National Environment Research Council equipment grant, in partnership with ESG, and was partially funded by the University of Liverpool and the Natural Sciences and Engineering Research Council of Canada (Discovery Grant to Young).

References

ASC (2003), *InSite Seismic Processor Users Manual*, Version 2.10, Applied Seismology Consultants, Ltd., Shrewsbury, UK.

Brace, W.F., Paulding, B.W., and Scholz, C. (1966), *Dilatancy in the fracture of crystalline rocks*, J. Geophys. Res. *71*, 3939–3953.

Lei, X.-L., Kusunose, K., Rao, M.V.M.S., Nishizawa, O., and Satoh, T. (2000), *Quasi-static fault growth and cracking in homogenous brittle rock under triaxial compression using acoustic emission monitoring*, J. Geophys. Res. *105*, 6127–6139.

Lei, X.-L., Kusunose, K., Satoh, T., and Nishizawa, O. (2003), *The hierachical rupture process of a fault: An experimental study*, Phys. Earth Planet. Inter. *137*, 213–228.

Lockner, D. A., Byerlee, J. D., Kuksenko, V., Ponomarev, A. and Sidorin, A. (1991), *Quasi-static, fault growth and shear fracture energy in granite*, Nature, 350, 39–42.

Lockner, D. A., Byerlee, J. D., Kuksenko, V., Ponomarev, A., and Sidorin, A., *Fault mechanics and transport properties of rocks* (eds. Evans, B., and Wong, T-F) (Academic, London 1992).

Lockner, D. A. and Byerlee, J. D., *Development of fracture planes during creep in granite*, in *Proceedings, Second Conference on Acoustic Emission/Microseismic Activity in Geological Structures and Materials* (eds. H. R. Hardy and W.F. Leighton) pp. 11–25 (Trans-Tech Publications, Clausthal- Zellerfeld, Germany 1980).

Main, I. G. and Meredith, P.G. (1989), *Classification of earthquake precursors from a fracture mechanics model*, Tectonophysics *167*, 273–283

Moore, D. E. and Lockner, D.A. (1995), *The role of microcracking in shear-fracture propagation in granite*, J. Struct. Geol. *17*, 95–114.

Mogi, K. (1962), *The influence of the dimensions of specimens on the fracture strength of rocks*, B. Earthquake Res. I, Tokyo, 40, 175–185.

Nelder, J. and Mead, R. (1965), *A simplex method for function minimization*, Computer J. *7*, 308–312.

Ohnaka, M. (2000), *A physical scaling relation between the size of an earthquake and its nucleation zone size*, Pure Appl. Geophys. *157*(11–12), 2259–2282.

Ohnaka, M., (2003), *A constitutive scaling law and a unified comprehension for frictional slip failure, shear fracture of intact rock, and earthquake rupture,* J. Geophys. Res. *108* Art. No. 2080.

Ohnaka, M. and Shen, L. F. (1999), *Scaling of the shear rupture process from nucleation to dynamic propagation: Implications of geometric irregularity of the rupturing surfaces*, J. Geophys. Res. *104*, 817–844.

Pettitt, W. S. (1998), *Acoustic emission source studies of microcracking in rock,* PhD, Keele University, UK.

Paterson, M.S. and Wong, T.-f., *Experimental Rock Deformation - The Brittle Field*, (Springer, New York 2005), 347 pp.

Reches, Z. and Lockner, D.A. (1994), *Nucleation and growth of faults in brittle rocks*, J. Geophys. Res. *99*, 18159–18173.

Reches, Z., (1999), *Mechanisms of slip nucleation during earthquakes*, Earth Planet. Sci. Lett. *170*, 475–486.

Rice, J. R., *The mechanics of earthquake rupture*, In *Physics of the Earth's Interior* (Proc. Int'l School of Physics "E. Fermi", course 78,) (Amsterdam, Italian Physical Society/North Holland Publ. Co. 1980).

Scholz, C. H. (1968a), *Microfracturing and the inelastic deformation of rock in compression*, J. Geophys. Res. *73*, 1417–1432.

Scholz, C. H. (1968b), *The frequency magnitude relation of micro-fracturing in rock and its relation to earthquakes*, Bull. Seismol. Soc. Am. *58*, 399–415.

SCHUBNEL,. A. BENSON, P., THOMPSON, B. D., HAZZARD, J., and YOUNG, R. P. (2006), *Quantifying damage, saturation and anisotropy in cracked rocks by inverting elastic wave velocities*, Pure Appl. Geophys. this volume.

STANCHITS, S. A., LOCKNER, D. A., and PONOMAREV, A. V. (2003), *Anisotropic changes in P-wave velocity and attenuation during deformation and fluid infiltration of granite*, Bull. Seismol. Soc. Am. *93*, 1803–1822.

TERADA, M., YANIGADANI, T., and Ehara, S., *AE Rate controlled compression test of rocks*. In *Proc. 3rd Conf on Acoustic Emission/Microseismic Activity in Geol Structures and Materials* (eds. Hardy, H.R. and Leighton F.W.) pp. 159–171 (Trans-Technical, Clausthal- Zellerfeld 1984).

THOMPSON, B. D, Young, R. P., Lockner, and D. A. (2005), *Observations of premonitory acoustic emission and slip nucleation during a stick slip experiment in smooth faulted Westerly granite*, Geophys. Res. Letts. *32*, L10304, doi:10.1029/2005GL022750.

VON SEGGERN, D. (1980), *A random stress model for seismicity statistics and earthquake prediction*, Geophys. Res. Letts. *7*, 637–640.

ZANG, A., WAGNER, F. C., STANCHITS, S., JANSSEN, C., and DRESEN, G. (2000), *Fracture process zone in granite*, J. Geophys. Res. *105*, 23651–23661.

(Received May 24, 2005, revised October 31, 2005, accepted November 7, 2005)
Published Online First: May 12, 2006